In-beam γ-ray spectroscopy of ^{38–42}S

E. Lunderberg, A. Gade, V. Bader, T. Baugher, D. Bazin, J. S. Berryman, B. A. Brown, D. J. Hartley, F. Recchia, S. R. Stroberg, D. Weisshaar, and K. Wimmer

Phys. Rev. C **94**, 064327 — Published 29 December 2016

DOI: 10.1103/PhysRevC.94.064327

In-beam γ-ray spectroscopy of $^{38-42}$S

E. Lunderberg,[1,2] A. Gade,[1,2] V. Bader,[1,2] T. Baugher,[1,2,*] D. Bazin,[1] J. S. Berryman,[1] B. A. Brown,[1,2] D. J. Hartley,[3] F. Recchia,[1,†] S. R. Stroberg,[1,2,‡] D. Weisshaar,[1] and K. Wimmer[4,1,§]

[1]*National Superconducting Cyclotron Laboratory, Michigan State University, East Lansing, Michigan 48824, USA*
[2]*Department of Physics and Astronomy, Michigan State University, East Lansing, Michigan 48824, USA*
[3]*Department of Physics, U.S. Naval Academy, Annapolis, Maryland 21402, USA*
[4]*Department of Physics, Central Michigan University, Mount Pleasant, Michigan 48859, USA*

(Dated: December 5, 2016)

The low-energy excitation level schemes of the neutron-rich $^{38-42}$S isotopes are investigated via in-beam γ-ray spectroscopy following the fragmentation of ^{48}Ca and ^{46}Ar projectiles on a ^{12}C target at intermediate beam energies. Information on $\gamma\gamma$ coincidences complemented by comparisons to shell-model calculations were used to construct level schemes for these neutron-rich nuclei. The experimental data are discussed in the context of large-scale shell-model calculations with the SDPF-MU effective interaction in the *sd*-*pf* shell. For the even-mass S isotopes, the evolution of the yrast sequence is explored as well as a peculiar change in decay pattern of the second 2^+ states at $N = 26$. For the odd-mass ^{41}S, a level scheme is presented that seems complete below 2.2 MeV and consistent with the predictions by the SDPF-MU shell-model Hamiltonian; this is a remarkable benchmark given the rapid shell and shape evolution at play in the S isotopes as the broken-down $N = 28$ magic number is approached. Furthermore, the population of excited final states in projectile fragmentation is discussed.

I. INTRODUCTION

Neutron-rich $N = 28$ isotones – comprising ^{48}Ca, ^{46}Ar, ^{44}S, and ^{42}Si – have provided much insight into the changes of the structure of nuclei encountered in the regime of large isospin. Evidence for a breakdown of the traditional $N = 28$ magic number resulted from the pioneering observation of low-lying quadrupole collectivity in ^{44}S [1, 2] and fueled the field of rare-isotope science in the quest to unravel the origin of shell and shape evolution in exotic nuclei with experimental programs worldwide.

The structure of the neutron-rich sulfur isotopes displays a variety of phenomena that are closely tied to shell evolution in exotic nuclei [3], with shape [4–6] and configuration coexistence [7–9] driving the properties of ^{44}S ($N = 28$) at low excitation energy. It is interesting to explore the evolution of the low-lying states as $N = 28$ is approached. It was pointed out by Utsuno *et al.* [3] that tensor-driven shell evolution plays a critical role in the rapid shape transitions that occur in the S and Si isotopic chains towards $N = 28$. These effects are included in the SDPF-MU effective shell-model interaction introduced in [3] and the resulting predictions for the ^{40,41,42}S level schemes will be tested in the present work. The sulfur isotopes between $N = 20$ and $N = 28$ have been studied with a variety of experimental techniques [10–20], however, information on the level schemes even at low excitation energy is still scarce. Beyond $N = 28$, very few excited states have been reported in the S isotopic chain [21, 22].

Gamma-ray spectroscopy following, for example, β decay [19], intermediate-energy Coulomb excitation [14], multinucleon transfer reactions [17, 18, 20], and projectile fragmentation [15, 16] provided a first, limited glimpse of the level structure of the neutron-rich S isotopes approaching $N = 28$ [23]. Here, we report on the in-beam γ-ray spectroscopy of $^{38-42}$S following the fragmentation of ^{46}Ar and ^{48}Ca intermediate-energy projectile beams on a C target in the center of the GRETINA γ-ray spectrometer [24]. Complementing the comparisons by Wang *et al.* [18] of S level schemes to shell-model calculations with the SDPF-U effective interaction [25], we compare our measurements with similar calculations based on the SDPF-MU Hamiltonian, which was constructed to describe the shell and shape evolution in the S and Si isotopic chains as $N = 28$ is approached [3].

II. EXPERIMENT

The measurements were performed at the Coupled Cyclotron Facility at the National Superconducting Cyclotron Laboratory [26] at Michigan State University.

The ^{46}Ar projectile beam was produced from a ^{48}Ca primary beam impinging upon a 1363 mg/cm^2 ^{9}Be production target and separated with a 240 mg/cm^2 Al degrader in the A1900 fragment separator [27]. The same production target was used to energy-degrade the ^{48}Ca primary beam in a separate setting. The total momentum acceptance of the separator was limited to

*Present address: Los Alamos National Laboratory, Los Alamos, New Mexico 87545, USA
†Present address: Dipartimento di Fisica e Astronomia "Galileo Galilei", Università degli Studi di Padova and INFN Padova, I-35131 Padova, Italy
‡Present address: TRIUMF, Vancouver, British Columbia V6T 2A3, Canada
§Present address: Department of Physics, The University of Tokyo, Hongo, Bunkyo-ku, Tokyo 113-0033, Japan

$\Delta p/p = 0.25\%$ for both projectile beams. In two separate runs, the projectile beams impinged upon a 149 mg/cm^2 glassy ^{12}C reaction target located at the pivot point of the S800 spectrograph [28]. The ^{46}Ar and ^{48}Ca beams had mid-target energies of 67.0 MeV/u and 66.7 MeV/u, respectively. The projectile-like reaction residues formed in the collision with the target were identified event-by-event with the focal-plane detection system of the S800 spectrograph and time-of-flight information involving plastic scintillators in the beam lines upstream of the reaction target. The magnetic rigidity of the S800 spectrograph was set to center the one-neutron pickup residues, ^{47}Ar [22] and ^{49}Ca [29], respectively. In the same settings, due to the large acceptance of the spectrograph, $^{40-43}$S and $^{38-40}$S, respectively, entered the S800 focal plane. The particle identification spectra correlating the energy loss of the reaction residues measured in the S800 ionization chamber and their time of flight are shown in Fig. 1; the various S isotopes can be cleanly separated. The statistics for ^{43}S were not sufficient to construct a level scheme and thus will not be discussed here. Most transitions observed in ^{43}S can be associated with γ rays previously reported in Ref. [12].

The reaction target was surrounded by the Gamma Ray Energy Tracking In-beam Nuclear Array (GRETINA) [24], consisting of seven detector modules, each containing four high-purity, 36-fold segmented, Germanium crystals. The GRETINA detectors were arranged to cover forward angles, with four detector modules located at 58° and three at 90° with respect to the beam axis. The 3-dimensional coordinates of the γ-ray interaction points within the GRETINA crystals were determined from the signal decomposition of the digitized traces read out from each segment. The first interaction point, assumed to correspond to the coordinate with the largest energy deposition, was used to deduce the γ-ray emission angle that is used in the event-by-event Doppler reconstruction of the γ rays emitted by the reaction products in flight. The spectra shown in this work employ addback, a procedure recovering the γ-ray energy of events scattered from one crystal into a neighbor [30].

In-beam detection efficiencies, taking into account the Lorentz boost, were determined with a GEANT4 simulation [31], with parameters adjusted to reproduce GRETINA's response to standard calibration sources at rest. These in-beam efficiencies were used to obtain the relative γ-ray intensities from recorded peak areas, as given in the tables in the next section. To determine $\gamma\gamma$ coincidence relationships for placement of transitions in level schemes, software cuts with appropriate background subtraction on γ-ray transitions in $\gamma\gamma$ coincidence matrices were used.

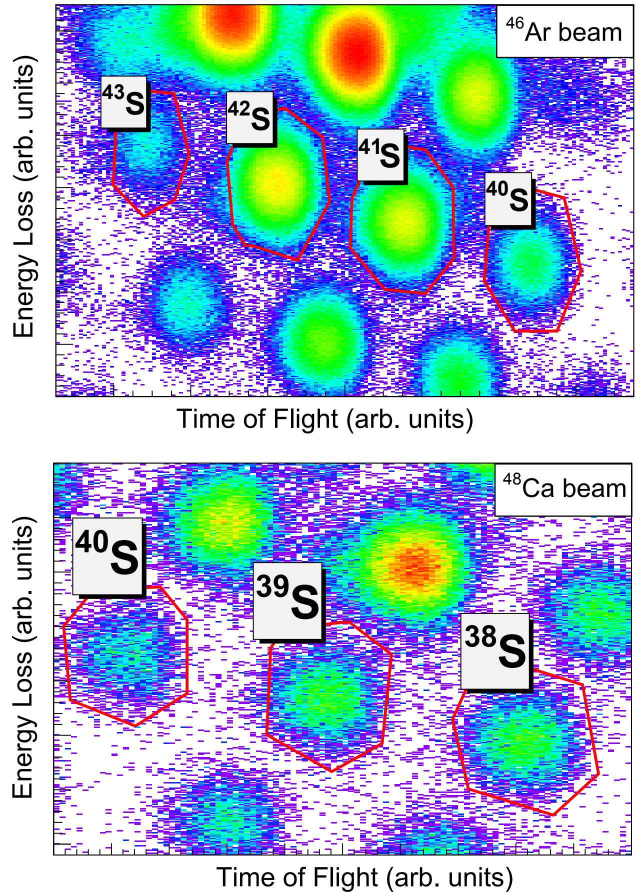

FIG. 1: Particle identification spectra for the reaction residues produced in ^{12}C(^{46}Ar,X)Y (upper panel) and ^{12}C(^{48}Ca,X)Y (lower panel). The energy loss was measured with the ionization chamber of the S800 focal plane. The time-of-flight was taken between plastic scintillators in the beam line and in the back of the S800 focal plane. The S isotopes of interest are unambiguously identified and separated.

III. RESULTS

In the following, we present our results for each isotope separately. The proposed level schemes are compared to large-scale shell-model calculations using the SDPF-MU [3] effective interaction for the sd-pf shell. The calculations adopted the full sd and fp model space for protons and neutrons, respectively, and used effective proton and neutron charges of $e_\pi = 1.35e$ and $e_\nu = 0.35e$ [3] and standard spin and orbital proton and neutron g factors. The calculations were carried out with the code NuShellX [32].

A. ^{38}S

Figure 2 shows the Doppler-reconstructed γ-ray spectrum taken in coincidence with ^{38}S reaction residues as produced in the fragmentation of the ^{48}Ca degraded primary beam. Several γ-ray transitions are present that will be discussed below.

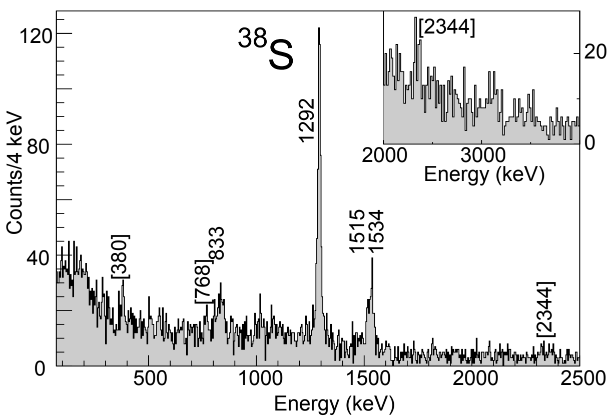

FIG. 2: Doppler-corrected ($v/c = 0.357$) γ-ray spectrum taken with GRETINA in coincidence with ^{38}S as identified with the S800 spectrograph. The inset expands the energy range from 2 to 4 MeV.

We observe strong transitions at 1292(4), 1515(6), and 1534(5) keV that can be identified with the previously reported $2_1^+ \rightarrow 0_1^+$, $(2_2^+) \rightarrow 2_1^+$ and $4_1^+ \rightarrow 2_1^+$ transitions, respectively [18, 20, 33–35]. This is consistent with the coincidence spectra shown in Fig. 3, where the small number of counts observed agrees with expectations based on the statistics in the singles spectrum and the detection efficiencies at the respective energies. Within our limited statistics, the 1515/1534 keV doublet is coincident with the 1292 keV $2_1^+ \rightarrow 0_1^+$ transition. No coincidence relationships could be established for the new, weaker γ-ray transitions.

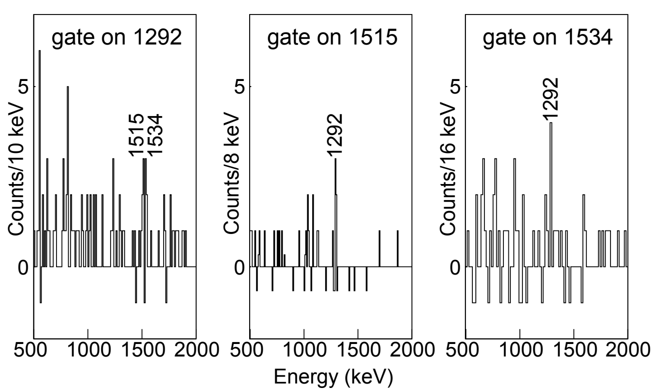

FIG. 3: Background-subtracted $\gamma\gamma$ coincidence spectra for ^{38}S. Coincidence spectra for the 1282, 1515, and 1534 keV transitions are shown. The small number of counts observed agrees with expectations based on the statistics of the measurement.

The 833(5) keV transition in our spectrum is 16 keV lower than the $(6_1^+) \rightarrow 4_1^+$ transition previously reported at 849 keV [18, 20]. Given the velocity of the S reaction residues, $v/c \sim 0.35$, and the C target thickness of 149 mg/cm^2, excited states with lifetimes of the order of several tens to hundreds of picoseconds will predominantly decay downstream of the target, signaled by a lowered peak energy and a left-tail in the Doppler-reconstructed γ-ray spectrum. The peak shape of the transition at 833 keV indeed seems to exhibit a left-tail in addition to the down shift in energy. GEANT simulations for different lifetime values reveal that the position and shape of the 833 keV transition is consistent with the emission of a 849 keV γ ray from a state that has a mean lifetime, τ, between 100 and 200 ps. Shell-model calculations with the SDPF-MU effective interaction, in fact, predict a lifetime for the 6_1^+ state of ~40 ps, which is an order of magnitude longer than the lifetime of the 2_1^+ state [35] but a factor of about 4 shorter than our estimate[1]. The association of the 833 keV transition reported here with the known 849 keV $(6_1^+) \rightarrow 4_1^+$ transition is plausible but would benefit from more statistics for conclusive $\gamma\gamma$ coincidence and line-shape analyses.

Table I lists the observed ^{38}S γ-ray energies together with their relative intensities and coincidence relationships. For the new weaker transitions reported here, coincidences could not be established due to low statistics.

TABLE I: Energies, intensities and coincidence relationships for γ-ray decays observed in ^{38}S. The 833(5) keV peak is significantly below the literature value of 849 keV, and has a peak shape indicative of a left tail. In comparison to simulations, both may be explained by a lifetime of 100 ps $< \tau <$ 200 ps. Transition energies placed in brackets indicate tentative identifications of γ-ray peaks.

E_γ [keV]	Rel. Intensities (%)	Coinc.
[380(5)]	5(1)	
[768(5)]	7(1)	
833(5)	25(3)	
1292(4)	100(10)	1515, 1534
1515(6)	10(2)	1292
1534(5)	29(4)	1292
[2344(9)]	10(2)	

Figure 4 compares the ^{38}S level scheme with the SDPF-MU shell-model calculations. The experimental scheme only contains the previously known transitions since the new γ rays reported here are too weak to be placed in the level scheme based on coincidence relationships. The weak transition at 380 keV may correspond to the

[1] Using the measured transition energy instead of the one from the shell model only increases the lifetime to 54 ps at constant $B(E2)$ strength.

383 keV transition visible in the ^{38}S spectrum of Wang *et al.* [18]. In their work as well as here, this γ ray remains unplaced. We note that the association of the 2807 keV level with the 2_2^+ state from the shell model is supported by the decay branching ratio. It is predicted within the SDPF-MU shell-model calculations that the $2_2^+ \rightarrow 2_1^+$ transition is the dominant decay branch with an intensity exceeding 96% of the total yield out of the 2_2^+ state. No evidence for a 2807 keV transition has been reported in any of the previous γ-ray spectroscopy measurements that observed the 1515 keV transition [20, 33] and there is no evidence for such a transition in the present work (see Fig. 2).

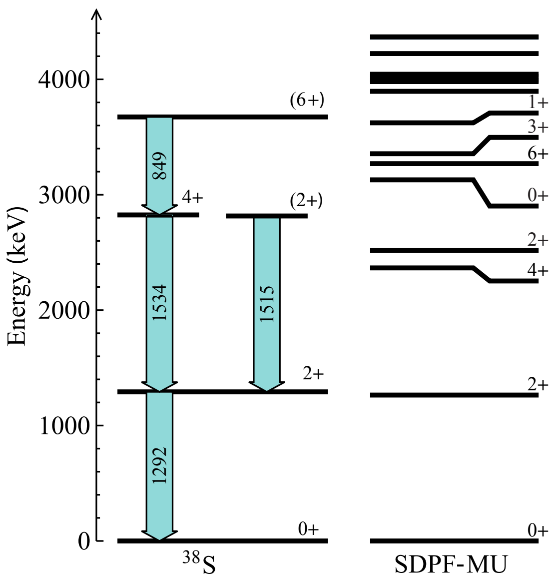

FIG. 4: Proposed experimental level schemes for ^{38}S based on previous data and coincidence relationships. The experimental level scheme is confronted with shell-model calculations using the SDPF-MU Hamiltonian.

Consistent with previous studies, transitions from yrast states are the most prominent in the γ-ray spectra of reaction residues from secondary fragmentation reactions with several nucleons removed from the projectile [36]. In the following, we will continue to explore this population pattern and use it to argue possible level schemes for the more exotic S isotopes.

B. ^{39}S

Figure 5 shows the Doppler-reconstructed γ-ray spectrum taken in coincidence with ^{39}S reaction residues produced in the projectile fragmentation of ^{48}Ca. The transitions at 337(4), 392(6), 466(4), 702(4), 1518(4), 1655(6), 1728(5) keV have been reported before from multinucleon transfer reactions [18, 38], β decay of ^{39}P [39], and ^{40}P βn emission [19]. We identify the 392(6) keV line with the 398 keV transition reported in the references above

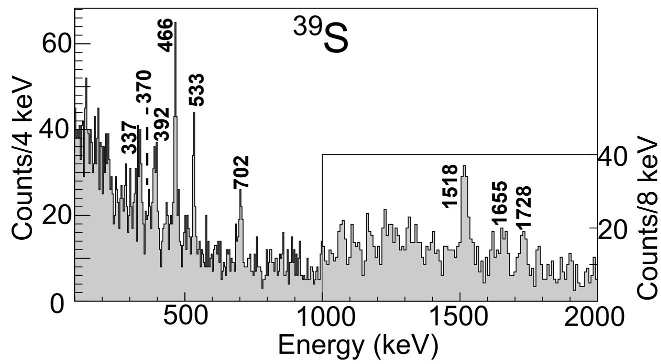

FIG. 5: Doppler-reconstructed γ-ray spectrum in coincidence with ^{39}S ($v/c = 0.348$). The inset expands the higher-energy region of the spectrum.

Coincidences of the 392, 337 and 466 keV transitions were reported from the β-decay work [19]. In our intensity and peak-to-background regime at low energies, weak evidence was seen only for the 337-466 keV coincidence (see Fig. 6). The two new transitions reported in this work, at 370(6) keV and 533(4) keV, appear to be in coincidence, with the 370 keV transition feeding the state that decays by emitting a 533 keV γ ray, based on intensity arguments.

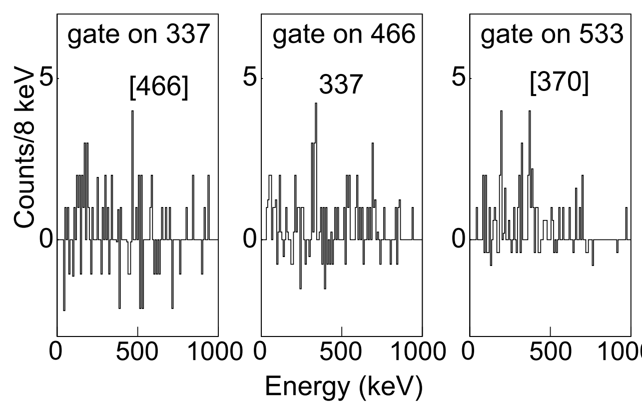

FIG. 6: Background-subtracted $\gamma\gamma$ coincidence spectra for ^{39}S. Software gates on the 337, 466, and 533 keV transitions are displayed. The coincidence spectra shown in the left and in the middle panel investigate the previously claimed 337-466 keV coincidence [19], which seems plausible based on our low-statistics data. The right panel provides weak evidence for a coincidence between the newly observed 533 and 370 keV transitions.

The transition energies, intensities, and coincidence relationships are summarized in Table II. We confirm previously reported γ-ray transitions and add two news ones at 370 and 533 keV that appear to be in coincidence.

TABLE II: Energies, intensities and coincidence relationships for γ-ray decays in ^{39}S.

E_γ [keV]	Rel. Intensities (%)	Coinc.
337(4)	28(5)	[466]
370(6)	9(3)	
392(6)	42(7)	
466(4)	71(10)	337
533(4)	38(7)	[370]
702(4)	42(8)	
1518(4)	100(15)	
1655(6)	59(11)	
1728(5)	43(9)	

From the present data on ^{39}S, it is hardly possible to propose a firm level scheme – this is not just due to the lack of coincidences but also related to the expected structure at low energies. The difficulty becomes apparent from the predicted level scheme displayed in Fig. 7. A triplet of states is expected within an energy range of $\sim$200 keV. Depending on the exact excitation energies, the two lowest-lying excited states may be nanosecond isomers, as predicted by the shell-model calculation. In-beam γ-ray spectroscopy at our beam velocities has limited sensitivity to nanosecond isomers. This makes it difficult to construct a level scheme since transitions or cascades can feed the ground state or any of the possible isomers.

Chapman *et al.* [38] propose a level scheme in comparison to shell-model calculations and $N = 23$ isotones, with 398- and 339-keV transitions depopulating the $(3/2^-_1)$ excited state to the $(7/2^-)$ ground state and the $(5/2^-_1)$ first-excited level at 59 keV. The $(3/2^-)$ is then suggested to be fed by the 466-keV decay of the first $(3/2^+)$ cross-shell excitation. While this is consistent with previously reported coincidence relationships, it would mean that, based on our intensities $I_\gamma(337) + I_\gamma(392) \approx I_\gamma(466)$, there is no room for any significant direct population or additional unobserved, discrete feeding of the $(3/2^-)$ level. The transitions reported here (Table II) are indeed indicative of positive-parity states, i.e. $3/2^+$ and $1/2^+$, located in the gap from 300 keV to 1600 keV that separates the first two groups of negative-parity states in ^{39}S (Fig. 7). The higher-energy transitions are likely connecting the second group of negative-parity states expected between 1.6 and 2 MeV to the first group near the ground state. The observed energies of 1518, 1655 and 1728 keV fit this picture well. Certainly, a firm level scheme for ^{39}S requires a measurement with sufficient statistics for $\gamma\gamma$ coincidences, and sensitivity to low-energy γ-ray transitions and isomers.

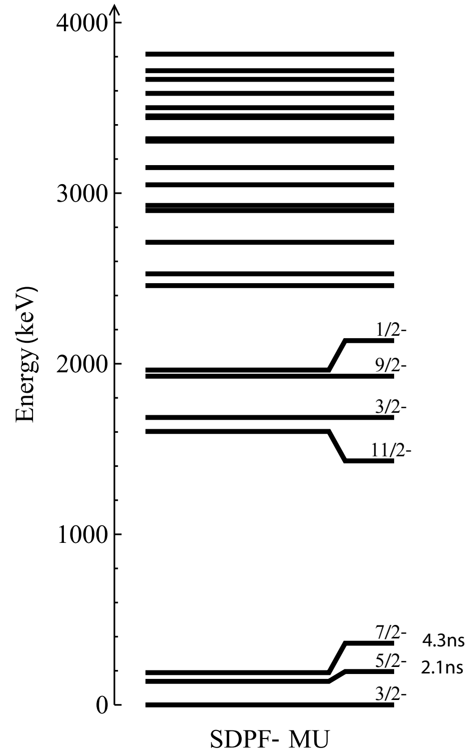

FIG. 7: Predicted level scheme and nanosecond lifetimes for ^{39}S from shell-model calculations using the SDPF-MU effective interaction.

C. ^{40}S

Figure 8 shows the Doppler-reconstructed γ-ray spectrum taken in coincidence with the ^{40}S reaction residues. ^{40}S was produced in the fragmentation of ^{48}Ca as well as from the ^{46}Ar projectile beam (see Fig. 1). The two data sets were added for the purpose of γ-ray spectroscopy. Previous information on the spectroscopy of ^{40}S stems from intermediate-energy Coulomb excitation [1], fragmentation [16], ^{40}P β decay [19], and most recently multinucleon transfer [18].

Nine γ-ray transitions are apparent in our spectrum. Compared to the β-decay work, the only common transitions are at 902 and 1350 keV [19]. This complementarity in the population pattern can most likely be attributed to the suspected $(2^-, 3^-)$ ground state of the β-decay parent and the resulting selective population of final states in the decay daughter. This is in contrast to the observation that fragmentation reactions seem to populate low-lying yrast states the strongest. Other overlapping transitions with previous work are 891(13) keV from intermediate-energy Coulomb excitation [1], 909(5) and 1356(6) keV from projectile fragmentation [16], and 904, 1352, and 1572 keV from multinucleon transfer [18].

In addition, $\gamma\gamma$ coincidence relations could be established for several transitions, as shown in Fig. 9. The

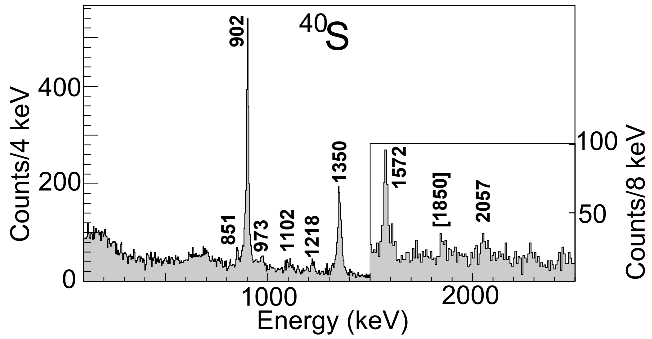

FIG. 8: Doppler-reconstructed γ-ray spectrum in coincidence with ^{40}S (with $v/c = 0.341$ for ^{40}S from ^{48}Ca beam and $v/c = 0.350$ for ^{40}S from ^{46}Ar beam).

coincidence spectra of the 902, 1350, and 1572 keV transitions show that they are mutually coincident, consistent with decaying to each other in a cascade. Weak evidence is visible in the spectrum gated on 1350 keV for a coincidence with the 2057 keV transition.

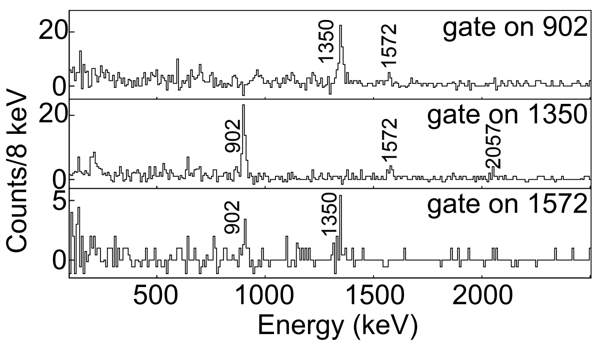

FIG. 9: Background-subtracted $\gamma\gamma$ coincidence spectra for ^{40}S. Spectra in coincidence with the strongest transitions at 902, 1350, and 1572 keV are shown.

The observed transition energies, intensities and coincidence relations are listed in Table III. It is clear from the coincidence spectra in Fig. 9 that the statistics in the 1572 keV line is just sufficient for a $\gamma\gamma$ coincidence analysis and, therefore, a placement of the weaker transitions reported here in the level scheme was not possible.

Figure 10 shows the experimental level scheme proposed in this work. Based on the coincidences and the γ-ray intensities reported here, see Fig. 9 and Table III, we propose the 1572 − 1350 − 902 keV cascade to correspond to the $(6_1^+) \rightarrow (4_1^+) \rightarrow 2_1^+ \rightarrow 0_1^+$ even-spin yrast sequence, consistent with Wang *et al.* [18]. Also, the 902, 1350 and 1572 keV transitions are the most intense in our spectrum, consistent with the population pattern reported in Section III.A for ^{38}S where the strongest transitions were the decays within the ground-state band up to the 6^+ state. The 2057 keV transition is placed tentatively as feeding the (4_1^+) state based on the spectrum in coincidence with the 1350 keV line.

TABLE III: Energies, efficiency-corrected relative intensities, and coincidence relations for γ-ray decays observed in ^{40}S. As for ^{38}S, the transitions suspected to form the even-spin yrast cascade are the most intense.

E_γ [keV]	Rel. Intensity (%)	Coinc.
851(4)	5(1)	
902(4)	100(8)	1350, 1572
973(4)	5(1)	
1102(6)	9(1)	
1218(4)	7(1)	
1350(4)	76(6)	902, 1572, 2057
1572(4)	20(2)	902, 1350
[1850(5)]	4(1)	
2057(6)	8(1)	

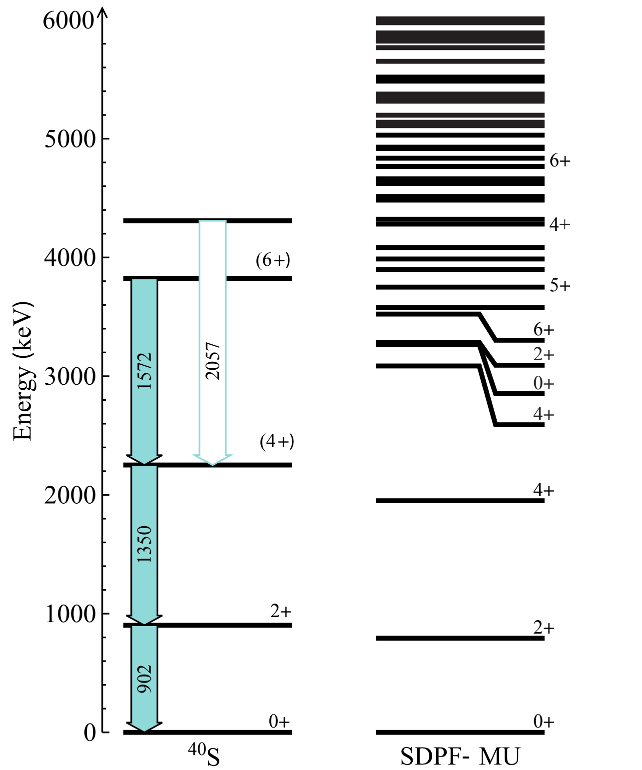

FIG. 10: Proposed experimental level scheme for ^{40}S compared to the SDPF-MU shell-model calculations. The level scheme is based on the $\gamma\gamma$ coincidence spectra and intensities. The tentative placement of the 2057 keV transition is indicated. The tentative identification of the low-lying even-spin yrast sequence is based on comparison with the shell model and the population pattern of excited states observed throughout this work.

We note that Winger *et al.* attribute the 1350 keV transition to the $(2_2^+) \rightarrow 2_1^+$ decay. This is at odds with our work and with the results from the multinucleon transfer [18] and the earlier projectile fragmentation measurement [16], where the 902 and 1350 keV transitions are attributed to the $2_1^+ \rightarrow 0_1^+$ and $(4_1^+) \rightarrow 2_1^+$ decays, respectively. We see no evidence for the 1013 keV γ ray that was tentatively proposed by Winger *et al.* to connect the yrast 4^+ and 2^+ states.

Shell-model calculations with the SDPF-MU effective interaction describe the even-spin yrast sequence of ^{40}S well as shown in the comparison in Fig. 10. The level density in ^{40}S is predicted to increase significantly at about 3 MeV. The many weak transitions not placed within the level scheme will originate from the multitude of states in this excitation energy region. Possible candidate states for the level established by the 2057 keV transition are higher-lying 4^+ or 6^+ states or the first 5^+ level (see Fig. 10).

D. ^{41}S

Figure 11 shows the Doppler-reconstructed γ-ray spectrum taken in coincidence with ^{41}S reaction residues produced in the fragmentation of ^{46}Ar projectiles. Sixteen γ-ray transitions are visible in the complex spectrum. Of these, transitions that likely correspond to our 451, 902, and 1613 keV γ-ray transitions have been previously observed in intermediate-energy Coulomb excitation [14] (449 and 904 keV), in β decay from ^{41}P [39] (904, 1308 and 1613 keV) and in multinucleon transfer [17] (449 keV).

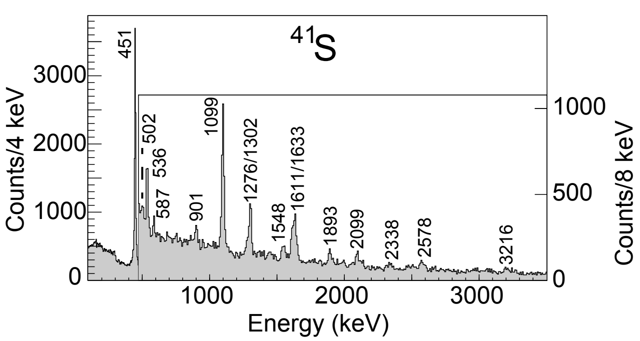

FIG. 11: Doppler-reconstructed γ-ray spectrum in coincidence with ^{41}S ($v/c = 0.342$). The spectrum is expanded with changed binning beyond 500 keV to highlight the high density of small peaks up to ∼3.2 MeV.

Our level of statistics allowed for a $\gamma\gamma$ coincidence analysis, as shown in Fig. 12, with several conclusive relationships established. In a software gate on the 451 keV line, 536, 1099 and 1633 keV transitions are clearly visible. The 536 keV transition is in coincidence with both 451 and 1099 keV and a gate on 1099 keV returns the 451 and 536 keV lines. The 1633 keV transition is cleanly observed only in coincidence with 451 keV. We note that the peak structure at ∼1620 keV is a doublet of two peaks with centroids of 1611 and 1633 keV, where a software gate on the right peak, mainly 1633 keV, returns the 451 keV while a gate on the lower-energy side, narrowly on 1611 keV, does not (see Fig. 13). Similarly, the 1302 keV transition is comparably intense and no coincidence is apparent, as shown in Fig. 13. The transition energies, intensities, and coincidence relationships are summarized in Table IV.

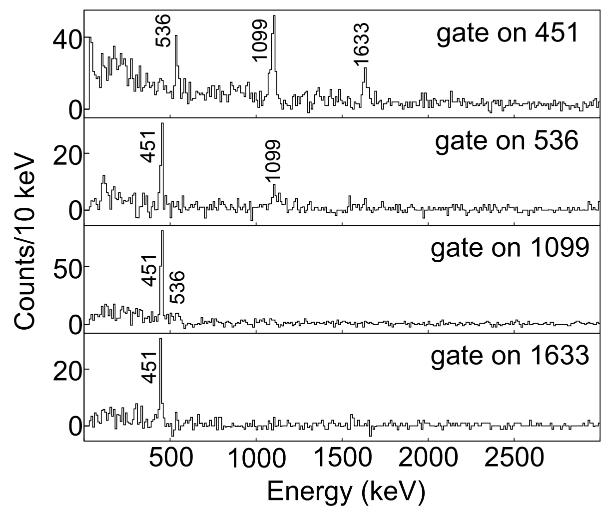

FIG. 12: Background-subtracted $\gamma\gamma$ coincidence spectra for ^{41}S. Spectra in coincidence with 451, 536, 1099, and 1633 keV are shown.

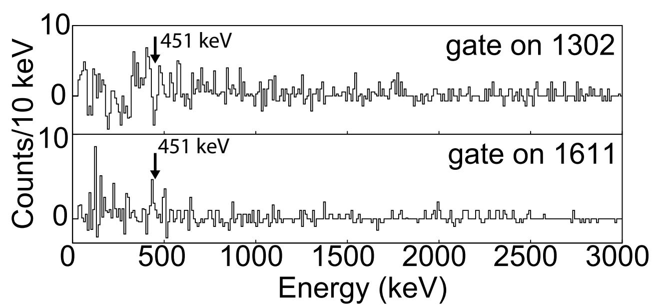

FIG. 13: Background-subtracted $\gamma\gamma$ coincidence spectra for ^{41}S. Spectra gated on 1611 and 1302 keV transitions in ^{41}S are shown. These transitions do not appear in coincidence with 451 keV (see also Fig. 12) or any other transitions that they would feed.

The proposed level scheme is shown in Fig. 14. The placement of the transitions is based on $\gamma\gamma$ coincidences, energy sums, and intensities observed in the present work.

Based on comparison between shell-model calculations and observed decay patterns, spin-parities of $(5/2^-)$,

TABLE IV: Energies, efficiency-corrected relative γ-ray intensities, and coincidences for ^{41}S.

E_γ [keV]	Rel. Intensity (%)	Coinc.
451(4)	100(6)	536, 1099, 1633
502(4)	1.0(2)	
536(4)	8.8(8)	451, 1099
587(4)	2.5(2)	
901(4)	4.8(4)	
1099(4)	41(3)	451, 536
1276(4)	4.2(5)	
1302(4)	13.4(1.2)	
1548(4)	7.3(8)	
1611(4)	11.5(1.1)	
1633(4)	19(2)	451
1893(4)	7.4(8)	
2099(5)	6.4(7)	
2338(6)	5.0(6)	
2578(5)	6.0(7)	
3216(8)	6.7(8)	

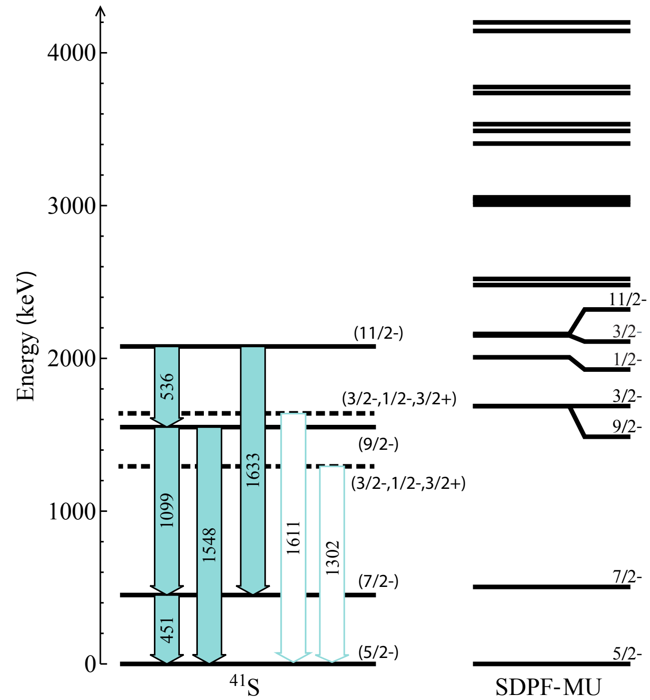

FIG. 14: Proposed experimental level schemes for ^{41}S based on the observed coincidences, intensities, energy sums and comparison to the shell model (SDPF-MU Hamiltonian). Solid lines and filled arrows indicate firm level and transition assignments, the dashed line and unfilled arrows indicate a tentative placement. Given that the 1611 and 1302 keV γ-ray transitions are strong and not in coincidence with 451 keV, we argue that they likely populate the ground state directly. Comparison to shell-model energies, decay branchings, and systematics was used to assign tentative J^π values (see text).

$(7/2^-)$, $(9/2^-)$, $(3/2^-, 1/2^-, 3/2^+)$ and $(11/2^-)$ are tentatively assigned to the lowest-lying states in our experimental level scheme. These assignments provide reasonable matches of measured and calculated excitation energies, and in addition, are supported by comparison of the measured and calculated decay patterns. The $9/2^-$ state is predicted to have a branching ratio of 83% to the $7/2^-$ state and 17% to the $5/2^-$ ground state. As listed in Table IV, the branching ratio for $(9/2^-)$ from our work is 85(2)% to the $(7/2^-)$ state and 15(2)% to the ground state. For the level that we tentatively identify as the $(11/2^-)$ state, the strongest decay leads to the $(7/2^-)$ state with 68(3)% of the total strength, and the remaining 32(3)% feeds the tentative $(9/2^-)$ state. The predicted branching ratios for these transitions are 69% and 31%, respectively, in good agreement with the data. Our $(3/2^-, 1/2^-, 3/2^+)$ assignments are based on the fact that the 1302 and 1611 keV γ rays are among the most intense transitions (see Table IV) while not being in coincidence with 451 keV or other strong transitions. We propose that both decay to the ground state directly, forming excited states at 1302(4) and 1611(4) keV. Comparison to the SDPF-MU shell-model calculations reveal the $3/2^-_1$ and $1/2^-_1$ states as the closest in energy with transitions to the ground state exceeding 97% of all de-excitations. The previous β-decay work offers support for this proposition. Winger *et al.* [39] report 1308 and 1614 keV γ rays that likely correspond to the 1302 and 1611 keV transitions observed in the present work. Our shell-model calculations with the SDPF-MU Hamiltonian suggest that the decay parent ^{41}P has a ground-state spin-parity of $1/2^+$ and a first excited $3/2^+$ state at 274 keV. Either of these possible J^π values for the ^{41}P ground state could populate the $1/2^-$ and $3/2^-$ states in ^{41}S, allowing their observation in [39]. If the $1/2^-$ and $3/2^-$ states were indeed at 1302 and 1611 keV, we would have observed all low-lying negative-parity states below 2.2 MeV consistent with the systematics of excited states populated in fragmentation. However, positive parity-states, corresponding to neutron cross-shell excitations across $N = 20$ as discussed for the Si isotopic chain [40], may be found at low excitation energy as well. A $3/2^+$ level would be expected to decay to the $(5/2^-)$ ground state and would have been strongly populated in the β decay of the positive-parity ground state. Such a positive-parity state is expected from systematics, but is based on cross-shell excitations and is therefore outside of the shell-model space employed here.

We show the shell-model level scheme up to 4 MeV and it is clear that the multitude of weaker, unplaced γ-ray transitions likely depopulate the higher-lying states. It is noted that our level scheme disagrees with the scheme proposed by Wang *et al.* [17] based on a low-statistics γ-ray singles spectrum obtained in multinucleon transfer. Wang *et al.* suggest that the 904 keV γ-ray transition reported in intermediate-energy Coulomb excitation [14], although they did not observe it in their own work, corresponds to the decay of the $9/2^-$ state to the ground state. This contradicts the expected decay pattern for such a state that would predominantly decay to the $7/2^-$ state.

Since multistep processes are severely suppressed in intermediate-energy Coulomb excitation [41], the observed γ rays in the work by Ibbotson *et al.* [14] were attributed to the depopulation of states at 449 and 904 keV, respectively. Based on a particle-rotor approach, the ground state and the proposed 449 and 904 keV levels were assigned $7/2^-$, $5/2^-$ and $9/2^-$ quantum numbers, respectively [14]. $M1$ excitations are heavily suppressed in Coulomb excitation and, in the absence of parity change, only $E2$ excitations have to be considered. In intermediate-energy Coulomb excitation, the proportionality between the excitation cross section and the $B(E\lambda; J_{gs} \rightarrow J_f)$ transition strength depends on the multipolarity, λ, but not explicitly on the spin values [41]. Therefore, we will refer to the $E2$ excitation strengths deduced by Ibbotson *et al.* as $B(E2\uparrow)$. Now, assuming the SDPF-MU shell-model spin and parity assignments, the $B(E2\uparrow)_{449\ \mathrm{keV}} = 167(65)\ e^2\mathrm{fm}^4$ and $B(E2\uparrow)_{904\ \mathrm{keV}} = 232(56)\ e^2\mathrm{fm}^4$ values from [14] have to be compared to $B(E2; 5/2^- \rightarrow 7/2^-) = 147\ e^2\mathrm{fm}^4$ and $B(E2; 5/2^- \rightarrow 9/2^-) = 59\ e^2\mathrm{fm}^4$, respectively. While the measured $B(E2)$ strength to the first excited state agrees well with the shell-model picture, all other calculated $B(E2)$ excitation strengths, including the one to the $9/2^-$ state, are expected to be smaller by a factor of 4 ($9/2^-_1$) or two orders of magnitude ($3/2^-_1$ and $1/2^-$) than what is reported for the $B(E2\uparrow)_{904\ \mathrm{keV}}$ value in [14]. While a very weak γ-ray transition at 902 keV is visible in our spectrum, it would be surprising if it corresponded to a low-lying state based on the population pattern of excited states in projectile fragmentation that we have observed so far. Ibbotson *et al.* explored the possibility of $E1$ excitations in their measurement and concluded that the measured cross sections would be beyond the recommended upper limits for $E1$ strength in the region but that this possibility of a parity-changing transition cannot be fully excluded [14].

Wang *et al.* further report a γ ray at 638 keV based on very low statistics and without coincidence data and assign it to connect the $11/2^-$ and the $7/2^-$ states. We see no evidence for a 638 keV transition in our ^{41}S spectrum.

The energies and γ-ray branching ratios of our level scheme agree with the shell-model calculation using the SDPF-MU effective interaction. The fact that we observe candidate states matching all calculated levels below 2.2 MeV is consistent with a picture where, with no discernible final-state selectivity, the lowest-lying states are the most prominent, likely populated directly in the reaction and fed indirectly through a multitude of higher-lying excited states that cascade toward the ground state.

E. ^{42}S

Figure 15 shows the Doppler-reconstructed γ-ray spectrum taken in coincidence with ^{42}S reaction residues resulting from the fragmentation of ^{46}Ar. More than 15 γ-ray transitions are identified in the spectrum. Of these transitions, only the 902 keV and 1820 keV γ rays have been reported before, in intermediate-energy Coulomb excitation (890(15) keV) [1] and in the fragmentation of a ^{48}Ca primary beam (904 and 1821 keV) [16]. Two γ-ray transitions, at 1466(8) keV and 1875(9) keV, reported in [16] are not observed in the present work.

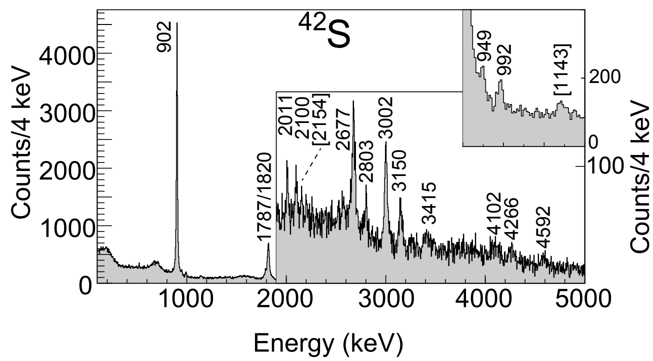

FIG. 15: Doppler-reconstructed γ-ray spectrum in coincidence with ^{42}S ($v/c = 0.335$). The insets expand energy regions of the spectrum with weaker intensity transitions. Transitions at 1143 and 2154 keV are tentative.

In addition, $\gamma\gamma$ coincidences were observed between several transitions, as shown in Figs. 16 and 17. First, the coincidence spectra for 902, 1787, and 1820 keV indicate that all three transitions are in coincidence with each other, forming a cascade that can be sorted by intensity. Furthermore, the 2100 keV transition is in coincidence with 902 keV and the 2803 keV γ-ray decay populates the state decaying by the 1820 keV transition.

An interesting structure emerges at high excitation energy. The background-subtracted coincidence spectrum for the weak 949 keV transition (see inset of Fig. 15) shows the 992 and 2677 keV transitions. A gate on the 992 keV line returns 902, 949 and 2677 keV transitions and shows a 992 keV self-coincidence that may point to a doublet structure. In coincidence with 2677 keV, all three transitions, 902, 949, and 992 keV, are visible.

The γ-ray transition energies, intensities and coincidence relationships are listed in Table V.

Based on $\gamma\gamma$ coincidences, intensities and energy sums, the level scheme shown in Fig. 18 is proposed. From the coincidence spectra of Fig. 16 and the intensities listed in Table V we propose the 1787 – 1820 – 902 keV cascade to correspond to the even-spin yrast sequence $(6^+) \rightarrow (4^+) \rightarrow 2^+ \rightarrow 0^+$. This is in reasonable agreement with the shell-model calculation where the biggest deviation is observed for the 6^+ state with the calculation placing

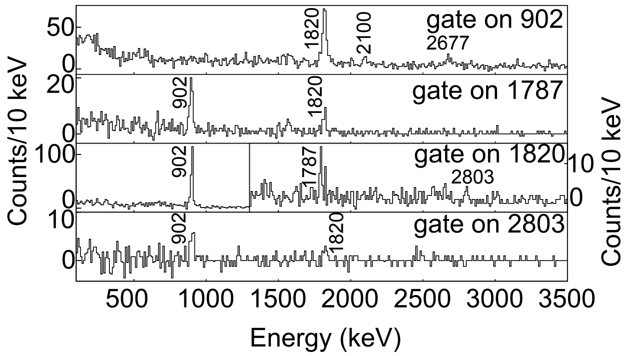

FIG. 16: Background-subtracted $\gamma\gamma$ coincidence spectra for ^{42}S. Spectra in coincidence with 902, 1787, 1820, and 2803 keV are shown.

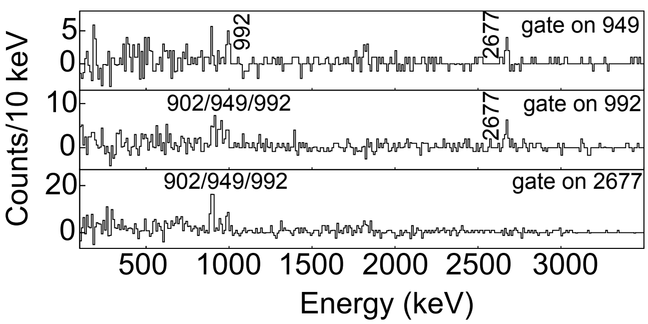

FIG. 17: Background-subtracted $\gamma\gamma$ coincidence spectra for ^{42}S. Spectra in coincidence with 949, 992, and 2677 keV are shown.

the state about 400 keV higher than the suggestion from experiment.

Placing the 2100 keV transition on top of the 2_1^+ state leads to a state at 3002(6) keV. In fact, we observe a 3002 keV γ-ray that then becomes a candidate to depopulate this new state directly to the ground state. We associate this state tentatively with the second 2^+ state of ^{42}S. The shell model predicts the 2_2^+ level at 3072 keV with a 84% branch to the ground state and the remaining 16% decaying to the 2_1^+ state. From our intensities in Table V we obtain a decay branching of 85(2)% to the ground state and 15(2)% to the 2_1^+ level. We note that our assignment is at odds with the level scheme proposed by Sohler *et al.* [16]. We do not observe the 1875 keV transition that is attributed in their work to depopulate the second 2^+ state to the first 2^+ state. Such a situation, where the $2_2^+ \rightarrow 0_1^+$ transition is not observed while the $2_2^+ \rightarrow 2_1^+$ is, would also be in contradiction to the shell-model calculations that have $2_2^+ \rightarrow 0_1^+$ as the strongest branch by a factor of five. We also observe no evidence for the 1466(8) keV γ-ray transition that establishes a 4245 keV state in ^{42}S in the work by Sohler *et al.* [16].

TABLE V: Energies, efficiency-corrected relative γ-ray intensities, and coincidences for ^{42}S. The 992 keV peak appears in coincidence with itself, suggesting that a doublet cannot be excluded for this transition.

E_γ [keV]	Rel. Intensity (%)	Coinc.
902(4)	100(6)	1820, 2100, 2677
949(4)	1.2(1)	992, 2677
992(6)	2.2(2)	902, 949, 992, 2677
[1143(4)]	1.6(2)	
1787(4)	8.4(7)	902, 1820
1820(4)	33(2)	902, 1787
2011(4)	2.2(3)	
2100(4)	1.8(2)	
[2154(4)]	0.9(1)	
2677(4)	10.6(9)	902, 949, 992
2803(4)	1.7(2)	902, 1820
3002(4)	10.1(9)	
3150(4)	5.4(6)	
3415(9)	5.1(5)	
4102(8)	5.2(6)	
4266(7)	3.1(4)	
4592(7)	2.9(4)	

The 2677 keV transition feeding the 2_1^+ state leads to a state at 3579(6) keV that, based on excitation energy alone, may be identified with the 3_1^+ state from the shell model or with a state from the group just above, comprising the 4_2^+, 3_2^+ and 0_2^+ states. From the decay pattern, however, the 3_1^+ and 4_2^+ levels are the only two with an essentially exclusive branch to the first 2^+ state. The 3_2^+ and 0_2^+ states are expected to exhibit significant decays to the second 2^+ state. A 3^- spin-parity assignment cannot be excluded and is outside of our shell-model configuration space.

From Fig. 17 and the intensities of Table V, we construct a cascade 949 – 992 – 2677 keV on top of the 2_1^+ state. This leads to two new excited states, at 4571(7) keV and 5520(8) keV. The 2803 keV transition that was found in coincidence with the (4_1^+) state now is a second branch of the new level at 5520 keV. Due to the high expected level density in this excitation energy region, it is not possible to associate this structure with states and decays of the SDPF-MU shell-model calculation. Many of the higher-lying 4^+ and 6^+ states, for example, show decay patterns broadly consistent with the high-lying structure in our level scheme.

IV. DISCUSSION

In Section III, we compare the ^{38,40,41,42}S level schemes from experiment to shell-model calculations with the SDPF-MU Hamiltonian. The motivation for choosing this shell-model effective interaction is rooted in its opti-

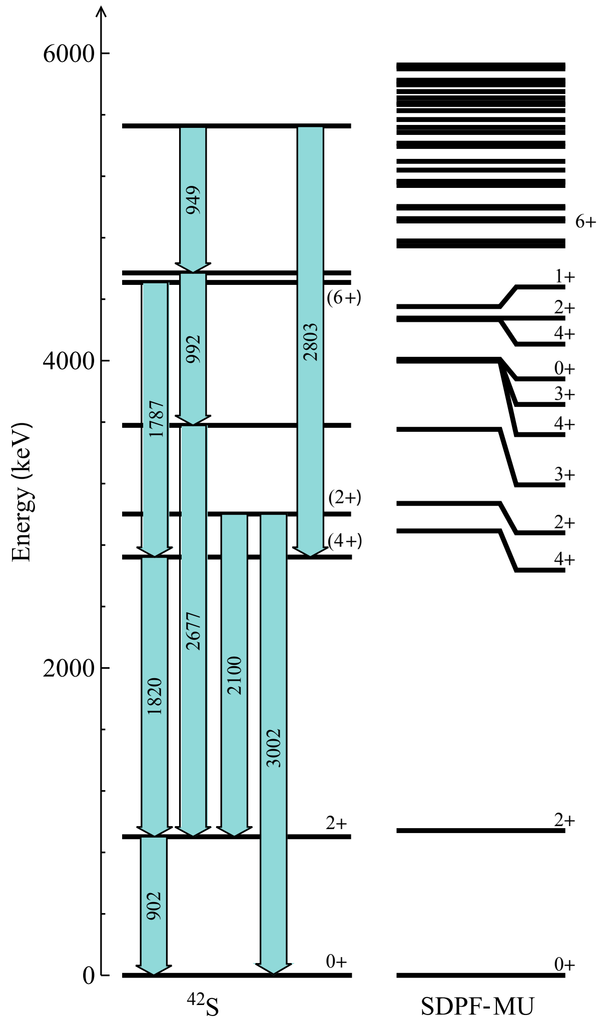

FIG. 18: Proposed experimental level scheme for ^{42}S based on the $\gamma\gamma$ coincidence spectra, intensities, and energy sums. The experimental data is confronted with shell-model calculations using the SDPF-MU effective interaction. Comparison to shell-model energies and decay branchings was used to assign tentative J^π quantum numbers (see text).

mization to explain the complex structure of the $N = 28$ isotones ^{42}Si and ^{44}S, comprising phenomena such as shape and configuration coexistence, on a common footing [3]. Furthermore, SDPF-U level schemes are available in the literature for ^{39}S [38], ^{40}S [18], and ^{41}S [17]. In contrast to SDPF-MU, the SDPF-U effective interaction consists of two parts, one valid for $Z \leq 14$ and one applicable to $Z \geq 15$ [25]. Earlier work benchmarked the performance of SDPF-MU in the chain of Si leading up to $N = 28$ [40] and the present work extends this comparison to the S isotopic chain. Below, (i) the character of the quadrupole collectivity of the even-mass S isotopes is considered from $E(4^+)/E(2^+)$ and $E(6^+)/E(2^+)$ energy ratios, (ii) the transition into the $N = 28$ "island of inversion" is characterized by an analysis of the decay properties of the 2_2^+ state, (iii) the odd-mass S isotopes are discussed, and the emerging pattern for the population of excited states in fragmentation reactions is summarized.

For even-even nuclei, the ratios of yrast excitation energies have long been used to classify collectivity in terms of vibrational, rotational, and transitional character. The chain of S isotopes, however, is challenging as shape and configuration coexistence is at play. We use $E(4_1^+)/E(2_1^+)$ and $E(6_1^+)/E(2_1^+)$ energy ratios to compare the ground-state bands of our proposed level schemes to the SDPF-MU shell-model calculations. Figure 19 shows the comparison of these ratios for the even-mass sulfur isotopes with $N = 20-28$. Assuming the 6_1^+ energies proposed in this work, good agreement is reached for the measured and calculated $E(6_1^+)/E(2_1^+)$ ratios in ^{38,40,42}S. For ^{36,44}S, the 6_1^+ state has not been identified in the literature. The systematics, which are not solely based on comparison with the shell model but also the population pattern of excited states that has emerged in this work, lend support to our new tentative 6_1^+ assignments for ^{40,42}S. For the $E(4_1^+)/E(2_1^+)$ ratio, close agreement is observed for ^{40,42}S while measurement and theory are only within $\sim$ 25% for the semi-magic ^{36}S and neighboring ^{38}S. It is noted that the shell-model calculation is not expected to work well for ^{36}S since the neutrons are restricted to the *sd* shell.

The case of ^{44}S is complex - a low-lying 4^+ state has been observed [7] that, based on two-proton knockout cross sections [7] and evidence for a long lifetime from a γ-ray line-shape analysis [7, 42], is suggested to correspond to a $K = 4$ isomer [7, 8]. This state differs in configuration from the 2_1^+ state, resulting in a strongly hindered $4_1^+ \rightarrow 2_1^+$ transition. The 4^+ level of ^{44}S that is connected to the collective 2_1^+ state [2] by a strong $E2$ decay has not yet been identified experimentally. With the intent of probing the collective nature of states with a similar underlying structure, we use the energies of the 4_2^+ shell-model state for ^{44}S since the corresponding cascade $6_1^+ \rightarrow 4_2^+ \rightarrow 2_1^+ \rightarrow 0_1^+$ is connected by the strongest $E2$ transitions. Using the 4_1^+ and 6_2^+ energies instead would not be noticeable in Fig. 19 as the energies of the first and second 4^+ and 6^+ states differ only by 56 and 134 keV, respectively. Future experiments will put the predictive power of the SDPF-MU shell-model Hamiltonian to the test once the collective structures beyond the first 2^+ state are identified in the complex nucleus ^{44}S whose low-lying structure is sensitively determined by shape and configuration coexistence.

An interesting systematic trend emerges for the 2_2^+ states in the S isotopic chain. According to the shell-model calculations with the SDPF-MU Hamiltonian, the second 2^+ state in ^{42}S has a unique structure that is reflected in the $2_2^+ \rightarrow 0_1^+$ and $2_2^+ \rightarrow 2_1^+$ branching ratio. For ^{38}S and ^{40}S, the $2_2^+ \rightarrow 2_1^+$ transitions are predicted to dominate with 96.4% and 99.4%, respectively. For ^{42}S, the branching is essentially reversed with 84% predicted for the $2_2^+ \rightarrow 0_1^+$ transition and only 16% for the $2_2^+ \rightarrow 2_1^+$ decay. The non-observation of the $2_2^+ \rightarrow 0_1^+$

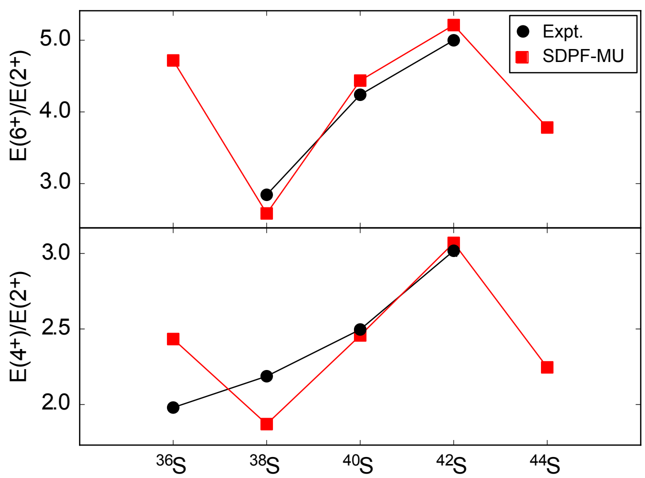

FIG. 19: Comparison of the excitation energy ratios of the first excited 2^+, 4^+, and 6^+ states across the neutron-rich sulfur isotopes. For ^{36}S, the 6_1^+ state has not yet been identified in the literature [23], and is expected at high excitation energy where the level density is significant. The collective 4^+ and 6^+ states of ^{44}S have not yet been observed either. For the calculated ^{44}S $E(4^+)/E(2^+)$ ratio, the shell-model energy of the second 4^+ state is used since the $6_1^+ \to 4_2^+ \to 2_1^+ \to 0_1^+$ cascade is connected by the strongest $E2$ transitions. However, the energy ratios would not change if the 4_1^+ or 6_2^+ energies were used instead since $E(6_2^+) - E(6_1^+) = 56$ keV and $E(4_2^+) - E(4_1^+) = 134$ keV. The tentative 6_1^+ assignments for ^{40,42}S stem from the measurements presented here.

branch in ^{38}S here and in [20] and the 85(2)% branch for $(2_2^+) \to 0_1^+$ in ^{42}S reported here are in remarkable agreement with this sudden structural change. We note that in ^{40}S the 2_2^+ level could not be identified — it is expected in a region of already high level density — and, solely based on energy, the 1850 keV γ ray may be a candidate for the 2_2^+ to 2_1^+ transition.

The reason for the abrupt change in the decay pattern of the 2_2^+ state in ^{42}S lies in its neutron single-particle structure. The 2_1^+ and 2_2^+ states in ^{42}S differ in the occupancies of the $0f_{7/2}$ and $1p_{3/2}$ neutron orbitals as detailed below. These two orbitals cannot be connected by the $M1$ magnetic dipole transition operator. Consequently, the $B(M1; 2_2^+ \to 2_1^+) \equiv B(M1)$ transition strength is strongly hindered with $B(M1) = 0.1355 \cdot 10^{-3}\ \mu_N^2$ in ^{42}S versus $B(M1) = 0.1924\ \mu_N^2$ in ^{40}S, disfavoring the $2_2^+ \to 2_1^+$ branch at $N = 26$. Figure 20 illustrates this by showing the occupancies of the neutron $1p_{3/2}$ orbital for the 0^+ (red) and 2^+ (blue) states up to 4.5 MeV from the calculations with the SDPF-MU Hamiltonian. Here, an increase of the neutron $1p_{3/2}$ occupancy is correlated with a decrease of the neutron $0f_{7/2}$ occupancy. The 2^+ state with the largest $1p_{3/2}$ occupancy is lowered in energy between ^{38}S and ^{42}S due to a reduction in the $1p_{3/2} - 0f_{7/2}$ single-particle gap as the neutron number increases. Up to ^{42}S, the configurations of the 0^+ and 2^+ states below 2 MeV are dominated by the $(a) = (0f_{7/2})^n$ configuration. The wave functions of the states above 2 MeV in ^{42}S are dominated by the $(b) = (0f_{7/2})^{(n-2)}(1p_{3/2})^2$ configuration[2]. Of all S isotopes shown, the neutron $p_{3/2}$ occupancy differs the most between the 2_1^+ and 2_2^+ states in ^{42}S, leading to the hindrance of the corresponding $2_2^+ \to 2_1^+$ $M1$ transition and the resulting very small $B(M1)$ value quoted above.

Figure 20 shows a dramatic change in the 0^+ and 2^+ level density below 4 MeV for ^{44}S and ties this to the excitation of neutrons across the $N = 28$ shell gap into the $p_{3/2}$ orbital. In ^{44}S, the correlation energy of the shell-breaking (b) configuration now becomes larger than that of the closed-shell configuration (a), putting ^{44}S inside the "island of inversion" at $N = 28$. The sensitivity of the $2_2^+ \to 2_1^+$ $M1$ decay to the $p_{3/2}$ neutron intruder occupancy now provides a very stringent test for the shell evolution leading up to the $N = 28$ "island of inversion". Our observation of a small $2_2^+ \to 2_1^+$ branch in ^{42}S, in agreement with the SDPF-MU calculations, indicates that this shell-model Hamiltonian indeed captures the changes in the neutron single-particle structure in the S isotopic chain as $N = 28$ is approached. It also illustrates how sudden the comparably simple structure of ^{42}S evolves into the complexity encountered for ^{44}S as the $N = 28$ shell closure breaks down.

For the odd-mass isotope ^{39}S, the expected low-lying nanosecond isomers, to which the present measurement is insensitive, prevent the construction of an experimental level scheme based on energy sums in the absence of clear coincidences and knowledge of the energies of the isomeric states. For ^{41}S on the other hand, the proposed experimental level scheme seems complete below 2.2 MeV and agrees remarkably well with the shell-model predictions. Given the complexity of the structure of the S isotopes, this agreement is noteworthy.

From all cases investigated here, a consistent picture emerges for the population of excited states in fragmentation reactions. Transitions from yrast states are the most prominent, visible even at low statistics (e.g. ^{38}S). For the higher statistics cases of ^{40,41,42}S, the presence of a multitude of weaker transitions can be understood as resulting from connections between the regions of high level density, upward from 3-4 MeV excitation energy, and the low-lying level scheme. While this may always have been the assumption behind the population of excited states in fragmentation reactions, evidence is presented here for the many feeding transitions that have remained unobserved in previous work discussing fragmentation reactions specifically for S isotopes [16] or the population of excited states in projectile-like fragmentation residues in general [36]. In the case of ^{41}S(^{42}S), all calculated nega-

---

[2] Due to the mixing of (a) and (b) and a small occupancy of the $0f_{5/2}$ and $1p_{1/2}$ orbitals, the change in the occupancy of the $p_{3/2}$ orbital is not exactly 2 between the two groups of states.

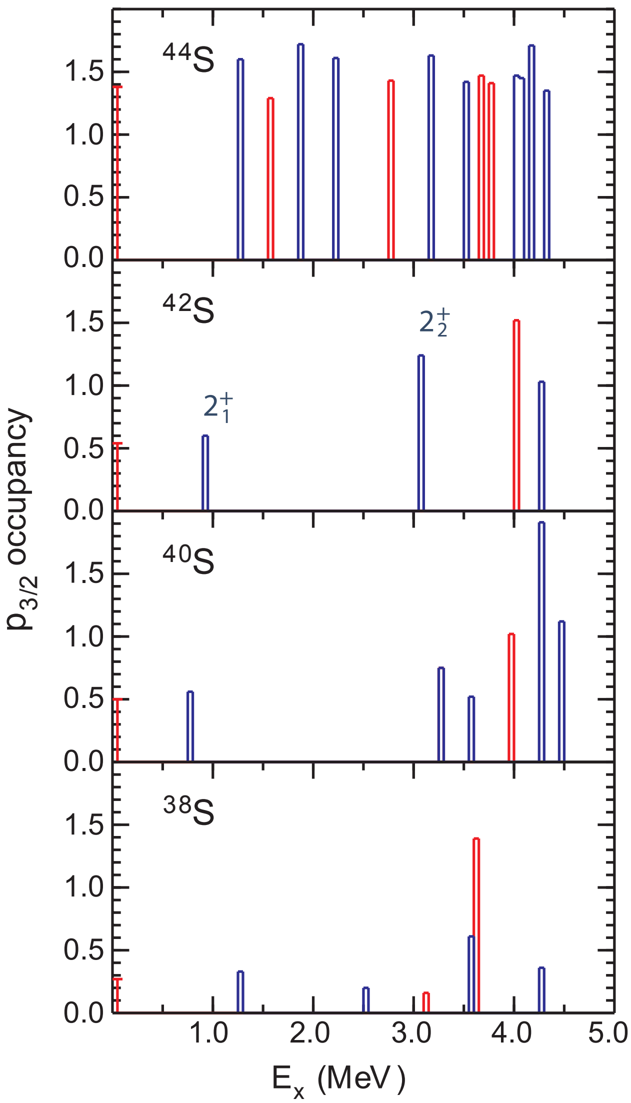

FIG. 20: Shell-model (SDPF-MU) neutron $p_{3/2}$ occupancy for the 0^+ (red) and 2^+ (blue) states of $^{38-44}$S below 4.5 MeV. The rapid onset of neutron $p_{3/2}$ occupancy together with the dramatic increase in the level density of 0^+ and 2^+ states in ^{44}S signals a sudden transition into the $N = 28$ "island of inversion" in the S isotopic chain. The role of ^{42}S as a sensitive probe for the neutron configurations is discussed in the text.

tive(positive) parity states below 2.2 MeV(3.5 MeV) have been matched to states in our proposed level schemes, including off-yrast states, while many weaker transitions remain unplaced. The prominence of yrast states can likely be attributed to their significant indirect feeding from the regions of high level density in addition to their direct population in the fragmentation reaction.

V. SUMMARY

We have performed in-beam γ-ray spectroscopy on neutron-rich sulfur isotopes populated by fragmentation of intermediate-energy ^{48}Ca and ^{46}Ar projectile beams. New transitions were identified in $^{39-42}$S and new level schemes for $^{40-42}$S are proposed from $\gamma\gamma$ coincidence information, energy sums and comparison to the shell model. Shell-model calculations with the SDPF-MU Hamiltonian provide remarkable agreement and consistency with the proposed level schemes. For the even-mass S isotopes, the evolution of the yrast sequence is discussed in terms of $E(6^+)/E(2^+)$ and $E(4^+)/E(2^+)$ energy ratios. For ^{42}S, a candidate for the 2^+_2 state is proposed that exhibits a unique decay pattern as compared to ^{38,40}S. This is rooted in its neutron single-particle structure and confirmed by the SDPF-MU shell-model calculations. For the odd-mass ^{41}S, a level scheme is presented that appears complete below 2.2 MeV and consistent with the predictions by SDPF-MU shell-model Hamiltonian; this is a remarkable benchmark given the rapid shell and shape evolution prevalent in this textbook isotopic chain as the diminished $N = 28$ shell gap is approached.

Acknowledgments

This work was supported in part by the National Science Foundation (NSF) under Contract No. PHY-1102511, by the US Department of Energy (DOE), Office of Nuclear Physics, under Grant No. DE-FG02-08ER41556, and by the DOE, National Nuclear Security Administration, under Award No. DE-NA0000979. GRETINA was funded by the DOE, Office of Science. Operation of the array at NSCL was supported by the NSF under Cooperative Agreement No. PHY-1102511 (NSCL) and DOE under Grant No. DE-AC02-05CH11231 (LBNL). B.A.B. acknowledges support from NSF Grant No. PHY-1404442. Figures 4, 7, 10, 14, 18 were created using the SciDraw scientific figure preparation system [43].

[1] H. Scheit, T. Glasmacher, B. A. Brown, J. A. Brown, P. D. Cottle, P. G. Hansen, R. Harkewicz, M. Hellström, R. W. Ibbotson, J. K. Jewell, K. W. Kemper, D. J. Morrissey, M. Steiner, P. Thirolf, and M. Thoennessen, Phys. Rev. Lett. **77**, 3967 (1996).

[2] T. Glasmacher, B.A. Brown, M.J. Chromik, P.D. Cottle, M. Fauerbach, R.W. Ibbotson, K.W. Kemper, D.J. Morrissey, H. Scheit, D.W. Sklenicka, and M. Steiner, Phys. Lett. **395**, 163 (1997).

[3] Y. Utsuno, T. Otsuka, B.A. Brown, M. Honma, T. Mizusaki, and N. Shimizu, Phys. Rev. C **86**, 051301 (2012).

[4] C. Force, S. Grevy, L. Gaudefroy, O. Sorlin, L. Caceres, F. Rotaru, J. Mrazek, N. L. Achouri, J. C. Angelique, F. Azaiez, B. Bastin, R. Borcea, A. Buta, J. M. Daugas, Z. Dlouhy, Zs. Dombradi, F. De Oliveira, F. Negoita, Y. Penionzhkevich, M. G. Saint-Laurent, D. Sohler, M. Stanoiu, I. Stefan, C. Stodel, and F. Nowacki, Phys. Rev. Lett. **105**, 102501 (2010).

[5] T.R. Werner, J.A. Sheikh, W. Nazarewicz, M.R. Strayer, A.S. Umar, and M. Misu, Phys. Lett. B **333**, 303 (1994).

[6] M.Kimura, Y.Taniguchi, Y.Kanada-Enyo, H.Horiuchi, K.Ikeda, Phys. Rev. C **87**, 011301 (2013).

[7] D. Santiago-Gonzalez, I. Wiedenhöver, V. Abramkina, M. L. Avila, T. Baugher, D. Bazin, B. A. Brown, P. D. Cottle, A. Gade, T. Glasmacher, K. W. Kemper, S. McDaniel, A. Rojas, A. Ratkiewicz, R. Meharchand, E. C. Simpson, J. A. Tostevin, A. Volya, and D. Weisshaar, Phys. Rev. C **83**, 061305(R) (2011).

[8] Y.Utsuno, N.Shimizu, T.Otsuka, T.Yoshida, Y.Tsunoda, Phys. Rev. Lett. **114**, 032501 (2015).

[9] J.L.Egido, M.Borrajo, T.R. Rodriguez, Phys. Rev. Lett. **116**, 052502 (2016).

[10] R. Chevrier, J.M. Daugas, L. Gaudefroy, Y. Ichikawa, H. Ueno, M. Hass, H. Haas, S. Cottenier, N. Aoi, K. Asahi, D.L. Balabanski, N. Fukuda, T. Furukawa, G. Georgiev, H. Hayashi, H. Iijima, N. Inabe, T. Inoue, M. Ishihara, Y. Ishii, D. Kameda, T. Kubo, T. Nanao, G. Neyens, T. Ohnishi, M.M. Rajabali, K. Suzuki, H. Takeda, M. Tsuchiya, N. Vermeulen, H. Watanabe, A. Yoshimi, Phys. Rev. Lett. **108**, 162501 (2012).

[11] L. Gaudefroy, J.M. Daugas, M. Hass, S. Grevy, Ch. Stodel, J.C. Thomas, L. Perrot, M. Girod, B. Rosse, J.C. Angelique, D.L. Balabanski, E. Fiori, C. Force, G. Georgiev, D. Kameda, V. Kumar, R.L. Lozeva, I. Matea, V. Meot, P. Morel, B.S. Nara Singh, F. Nowacki, G. Simpson, Phys. Rev. Lett. **102**, 092501 (2009).

[12] L.A. Riley, P. Adrich, T.R. Baugher, D. Bazin, B.A. Brown, J.M. Cook, P.D. Cottle, C.Aa. Diget, A. Gade, D.A. Garland, T. Glasmacher, K.E. Hosier, K.W. Kemper, A. Ratkiewicz, K.P. Siwek, J.A. Tostevin, D. Weisshaar, Phys. Rev. C **80**, 037305 (2009).

[13] R. Ringle, C. Bachelet, M. Block, G. Bollen, M. Facina, C.M. Folden III, C. Guenaut, A.A. Kwiatkowski, D.J. Morrissey, G.K. Pang, A.M. Prinke, J. Savory, P. Schury, S. Schwarz, C.S. Sumithrarachchi, Phys. Rev. C **80**, 064321 (2009).

[14] R. W. Ibbotson, T. Glasmacher, P. F. Mantica, and H. Scheit, Phys. Rev. C **59**, 642 (1999).

[15] F. Azaiez, M. Belleguic, D. Sohler, M. Stanoiu, Zs. Dombradi, O. Sorlin, J. Timar, F. Amorini, D. Baiborodin, A. Bauchet, F. Becker, C. Borcea, C. Bourgeois, Z. Dlouhy, C. Donzaud, J. Duprat, D. Guillemaud-Mueller, F. Ibrahim, M.J. Lopez, R. Lucas, S.M. Lukyanov, V. Maslov, J. Mrazek, C. Moore, F. Nowacki, B.M. Nyako, Yu.-E. Penionzhkevich, M.G. Saint-Laurent, F. Sarazin, J.A. Scarpaci, G. Sletten, C. Stodel, M. Taylor, C. Theisen, G. Voltolini, Eur. Phys. J. A **15**, 93 (2002).

[16] D. Sohler, Zs. Dombradi, J. Timar, O. Sorlin, F. Azaiez, F. Amorini, M. Belleguic, C. Bourgeois, C. Donzaud, J. Duprat, D. Guillemaud-Mueller, F. Ibrahim, J.A. Scarpaci, M. Stanoiu, M.J. Lopez, M.G. Saint-Laurent, F. Becker, F. Sarazin, C. Stodel, G. Voltolini, S.M. Lukyanov, V. Maslov, Yu.-E. Penionzhkevich, M. Girod, S. Peru, F. Nowacki, G. Sletten, R. Lucas, C. Theisen, D. Baiborodin, Z. Dlouhy, J. Mrazek, C. Borcea, A. Bauchet, C.J. Moore, M.J. Taylor, Phys. Rev. C **66**, 054302 (2002).

[17] Z.M. Wang, R. Chapman, F. Haas, X. Liang, F. Azaiez, B.R. Behera, M. Burns, L. Corradi, D. Curien, A.N. Deacon, Zs. Dombradi, E. Farnea, E. Fioretto, A. Gadea, A. Hodsdon, F. Ibrahim, A. Jungclaus, K. Keyes, V. Kumar, A. Latina, N. Marginean, G. Montagnoli, D.R. Napoli, J. Ollier, D. O'Donnell, A. Papenberg, G. Pollarolo, M.-D. Salsac, F. Scarlassara, J.F. Smith, K.M. Spohr, M. Stanoiu, A.M. Stefanini, S. Szilner, M. Trotta, D. Verney, Phys. Rev. C **83**, 061304 (2011).

[18] Z.M. Wang, R. Chapman, X. Liang, F. Haas, F. Azaiez, B.R. Behera, M. Burns, E. Caurier, L. Corradi, D. Curien, A.N. Deacon, Zs. Dombradi, E. Farnea, E. Fioretto, A. Gadea, A. Hodsdon, F. Ibrahim, A. Jungclaus, K. Keyes, V. Kumar, A. Latina, S. Lunardi, N. Marginean, G. Montagnoli, D.R. Napoli, F. Nowacki, J. Ollier, D. O'Donnell, A. Papenberg, G. Pollarolo, M.-D. Salsac, F. Scarlassara, J.F. Smith, K.M. Spohr, M. Stanoiu, A.M. Stefanini, S. Szilner, M. Trotta, D. Verney, Phys. Rev. C **81**, 054305 (2010).

[19] J.A. Winger, P.F. Mantica, R.M. Ronningen, M.A. Caprio, Phys. Rev. C **64**, 064318 (2001).

[20] B. Fornal, R. H. Mayer, I. G. Bearden, Ph. Benet, R. Broda, P. J. Daly, Z. W. Grabowski, I. Ahmad, M. P. Carpenter, P. B. Fernandez, R. V. F. Janssens, T. L. Khoo, T. Lauritsen, E. F. Moore, and M. Drigert, Phys. Rev. C **49**, 2413 (1994).

[21] A. Gade, P. Adrich, D. Bazin, B.A. Brown, J.M. Cook, C. Aa. Diget, T. Glasmacher, S. McDaniel, A. Ratkiewicz, K. Siwek, and D. Weisshaar, Phys. Rev. Lett. **102**, 182502 (2009).

[22] A. Gade, J. A. Tostevin, V. Bader, T. Baugher, D. Bazin, J. S. Berryman, B. A. Brown, C. Aa. Diget, T. Glasmacher, D. J. Hartley, E. Lunderberg, S. R. Stroberg, F. Recchia, A. Ratkiewicz, D. Weisshaar, and K. Wimmer, Phys. Rev. C **93**, 054315 (2016).

[23] Evaluated Nuclear Structure Data File (ENSDF), `http://www.nndc.bnl.gov/ensdf`.

[24] S. Paschalis *et al.*, Nucl. Instrum. Methods Phys. Res., Sect A **709**, 44 (2013).

[25] F. Nowacki and A. Poves, Phys. Rev. C **79**, 014310 (2009).

[26] A. Gade and B. M. Sherrill, Phys. Scrip. **91**, 053003 (2016).

[27] D. J. Morrissey *et al.*, Nucl. Instrum. Methods in Phys. Res. B **204**, 90 (2003).

[28] D. Bazin *et al.*, Nucl. Instrum. Methods in Phys. Res. **B 204**, 629 (2003).

[29] A. Gade, J. A. Tostevin, V. Bader, T. Baugher, D. Bazin, J. S. Berryman, B. A. Brown, D. J. Hartley, E. Lunderberg, F. Recchia, S. R. Stroberg, Y. Utsuno, D. Weisshaar, and K. Wimmer, Phys. Rev. C **93**, 031601(R) (2016).

[30] D. Weisshaar, D. Bazin, P. C. Bender, C. M. Campbell, F. Recchia, V. Bader, T. Baugher, J. Belarge, M. P. Carpenter, H. L. Crawford, M. Cromaz, B. Elman, P. Fallon, A. Forney, A. Gade, J. Harker, N. Kobayashi, C. Langer, T. Lauritsen, I. Y. Lee, A. Lemasson, B. Longfellow, E. Lunderberg, A. O. Macchiavelli, K. Miki, S. Momiyama, S. Noji, D. C. Radford, M. Scott, J. Sethi, S. R. Stroberg, C. Sullivan, R. Titus, A. Wiens, S. Williams, K. Wimmer, S. Zhu, Nucl. Instrum. Methods in Phys. Res. A, submitted (2016).

[31] L.A. Riley. UCGretina GEANT4. Ursinus College (unpublished).
[32] NuShellX, http://www.garsington.eclipse.co.uk/
[33] J. W. Olness, E. K. Warburton, J. A. Becker, D. J. Decman, E. A. Henry, L. G. Mann, and L. Ussery Phys. Rev. C **34**, 2049 (1986).
[34] E. K. Warburton, D. E. Alburger, and G. Wang, Phys. Rev. C **36**, 429 (1987).
[35] J.A. Cameron, B. Singh, *Nucl. Data Sheets* **109**, 1 (2008).
[36] A. Obertelli, A. Gade, D. Bazin, C. M. Campbell, J. M. Cook *et al.*, Phys. Rev. C **73**, 044605 (2006).
[37] S. Szilner, L. Corradi, F. Haas, G. Pollarolo, L. Angus *et al.*, Phys. Rev. C **87**, 054322 (2013).
[38] R. Chapman, Z. M. Wang, M. Bouhelal, F. Haas, X. Liang *et al.*, Phys. Rev. C **94**, 024325 (2016).
[39] J.A. Winger, *et al.*, Proc. Conf on Exotic Nuclei and Atomic Masses, Bellaire, Michigan, June 23-27, 1998; AIP Conf. Proc. 455, p.606 (1998).
[40] S. R. Stroberg, A. Gade, J. A. Tostevin, V. M. Bader, T. Baugher, D. Bazin, J. S. Berryman, B. A. Brown, C. M. Campbell, K. W. Kemper, C. Langer, E. Lunderberg, A. Lemasson, S. Noji, T. Otsuka, F. Recchia, C. Walz, D. Weisshaar, and S. Williams, Phys. Rev. C **91**, 041302(R) (2015).
[41] A. Winther and K. Alder, Nucl. Phys. A 319, 518 (1979).
[42] L. A. Riley, P. Adrich, N. Ahsan, T. R. Baugher, D. Bazin, B. A. Brown, J. M. Cook, P. D. Cottle, C. Aa. Diget, A. Gade, T. Glasmacher, K. E. Hosier, K. W. Kemper, A. Ratkiewicz, K. P. Siwek, J. A. Tostevin, A. Volya, and D. Weisshaar, Phys. Rev. C 86, 047301 (2012).
[43] M. A. Caprio, Comput. Phys. Commun. 171, 107 (2005).